Mohammad Sharifi Ghazijahani*, Christian Kästner, Valentina Valori,
Alexander Thieme, Kerstin Täschner, Jörg Schumacher and Christian Cierpka

The SCALEX facility – an apparatus for scaled fluid dynamical experiments

https://doi.org/10.1515/teme-2022-0121
Received December 16, 2022; accepted January 26, 2023
published online February 10, 2023

Abstract: The working conditions of the Scaled Convective Airflow Laboratory Experiment (SCALEX) at Technische Universität Ilmenau and sample experiments are reported. The SCALEX facility is a pressure vessel which allows for downscaling of laboratory experiments up to a factor of 20 by compression of gaseous working fluids, air or sulfur hexafluoride, to change the material properties of the fluid. The requirements and conditions for downscaling of fluid dynamical problems are discussed in detail. Long-term high and low pressure tests are conducted to screen the stability of the experimental environment inside the vessel against pressure and temperature fluctuations. Finally, a Rayleigh–Bénard convection experiment at an aspect ratio 10 is performed inside the SCALEX facility as a proof of concept. The reference experiment was conducted under 4.5 bar pressure for $\mathrm{Ra} = 1.9 \times 10^5$. However, the Rayleigh number could be varied in a wide range of $\mathrm{Ra} = 10^4 \ \dots \ 10^8$. The flow investigation was pursued with stereoscopic particle image velocimetry in horizontal mid-plane through the convection cell. To improve the image quality the cameras were placed inside the pressure cell and tested up to 6 bar. Thus the feasibility of optical flow measurements at elevated pressures is shown.

***Corresponding author: Mohammad Sharifi Ghazijahani**, Institute of Thermodynamics and Fluid Mechanics, Technische Universität Ilmenau, P. O. Box 100565, 98693 Ilmenau, Germany,
E-mail: mohammad.sharifi-ghazijahani@tu-ilmenau.de.
https://orcid.org/0000-0001-5885-4138
Christian Kästner, **Valentina Valori**, **Alexander Thieme**, **Jörg Schumacher and Christian Cierpka**, Institute of Thermodynamics and Fluid Mechanics, Technische Universität Ilmenau, P. O. Box 100565, 98693 Ilmenau, Germany
Kerstin Täschner, Fraunhofer Institute for Organic Electronics, Electron Beam and Plasma Technology FEP Dresden, Winterbergstraße 28, 01277 Dresden, Germany

Keywords: scaled experiments; SF_6; thermal convection; turbulence.

1 Introduction

Similar conditions at all scales have to be established when experiments in scaled models are compared with their real counterparts. Hence the boundary conditions of scaled experiments, e.g. the temperature difference between a heating and a cooling plate or the physical properties of the fluid, have to be adjusted according to the scale. This adjustment can be achieved by the use of the similarity theory. Thus, the flow can be characterized by a set of dimensionless numbers Π_i ($i = 1, 2, \dots, p$), where p is the size of the set of dimensionless numbers, which are required to describe the flow. A dimensionless number is usually the product of physical variables characterizing the flow. The least set size of dimensionless numbers $\Pi_{p,\min}$, fully describing the flow, can be determined by the Π-theorem, which was introduced by Buckingham in 1914 [1]. To set up the Π-theorem, it is necessary to figure out which physical variables affect the flow. The relevant variables for natural thermal convection, e.g. Rayleigh–Bénard convection, are the applied temperature difference ΔT between the hot and cold plates at the bottom and top of an infinitely extended fluid layer of height h, the acceleration due to gravity g and the working fluid properties, i.e. density ρ, dynamic viscosity η and volume expansion coefficient β. Thus a mathematical-physical description can be found:

$$f\left(\Delta T, h, g, \rho, \eta, \beta\right) = 0. \tag{1}$$

Based on the assumption that the temperature difference in the flow is small and that the Boussinesq approximation is valid, it is possible to neglect the temperature and pressure dependency of all material parameters. Quantities ν, c_p, λ, β, and ρ, and thus $\alpha = \lambda/(\rho c_p)$ are taken as constants [2]. Finally, there are $n = 6$ characteristic physical variables describing the flow, whereas these variables can be described by $k = 4$ fundamental physical quantities: time, mass, length and temperature. Hence the minimum number

of dimensionless numbers characterizing the flow in free thermal convection in an infinitely extended layer can be determined by the following equation:

$$p = n - k = 6 - 4 = 2. \tag{2}$$

The resulting two dimensionless numbers for describing thermally driven free convection are the Prandtl (Pr) and Rayleigh (Ra) number:

$$\mathrm{Pr} = \frac{\nu}{\alpha} = \frac{\eta}{\rho\alpha}, \tag{3}$$

$$\mathrm{Ra} = \frac{g\beta(T_H - T_C)L^3}{\nu\alpha} = \frac{\rho^2 g\beta(T_H - T_C)L^3 c_p}{\eta\lambda}. \tag{4}$$

Where ρ is the density of the fluid, ν the kinematic viscosity, η the dynamic viscosity, α the thermal diffusivity, g the acceleration due to gravity, β the thermal expansion coefficient, L the characteristic linear dimension, c_p the heat capacity at constant pressure, λ the thermal conductivity, T_H the bottom temperature and T_C the top-plate temperature.

The Rayleigh number Ra, which can be regarded as the relation between buoyancy and damping forces, can be applied to characterize the thermal convection. The Prandtl number Pr depicts the ratio between momentum diffusivity and thermal diffusivity.

A further dimensionless number, characterizing the geometrical dependency of a convection flow experiment, is the aspect ratio Γ, meaning the ratio of the lateral extension l and the height h of the convection cell:

$$\Gamma = \frac{l}{h}. \tag{5}$$

The aspect ratio parameter cannot be obtained by the dimensional analysis from above. Note that $L = h$, cf. Eq. (4). It is necessary since a laboratory experiment has to be conducted in a closed volume. Furthermore, the obtained structures change with aspect ratio as the boundary conditions at the side walls are more important for low Γ. In order to fully characterize the volume it is necessary to specify every main aspect ratio, i.e. for a rectangular box in direction of the width and the length of the box. Therefore, the dimensionless numbers provide a generalized characterization of the flow, e.g. whether the flow is turbulent or not. But they also allow for comparing flows. Such a comparison is very important since similar flows in a small-scale model experiment and reality can be achieved if the full set of dimensionless numbers agrees in both, experiment (I) and reality (II):

$$\frac{\Pi_{\mathrm{I},i}}{\Pi_{\mathrm{II},i}} = 1. \tag{6}$$

$\Pi_{\mathrm{I},i}$ and $\Pi_{\mathrm{II},i}$ are the sets of dimensionless numbers of the experiment and the reality, respectively. Hence this equation is the fundamental definition of the similarity theory. As already mentioned, the similarity between experiment and reality can only be achieved by adjusting the physical variables of the experiment to equal the dimensionless numbers to the reality. Thus there is only partial similarity achieved if the minimal set of dimensionless numbers does not satisfy the similarity equation [3]. Among the comparison between experiment and reality, the similarity theory also allows for comparison of results from different independent experimental and numerical studies of fluid mechanical problems. In general, it supports the adjustment of the boundary conditions of small-scale experiments with respect to full-scale problems. Hence the similarity theory is the basis for application of found results in small-scale experiments to reality or numerical simulations.

In this paper we want to discuss the working conditions of the Scaled Convective Airflow Laboratory Experiment (SCALEX) facility at Technische Universität Ilmenau, as well as a sample experiment on Rayleigh–Bénard convection. Therefore, the purpose of this paper will be to describe the extent to which SCALEX can provide the desired experimental parameters for Rayleigh–Bénard convection so that experiments comparable to reality can be conducted. The results of a reference experiment for $\mathrm{Ra} = 1.9 \times 10^5$ will be shown at the end.

2 Rayleigh–Bénard convection and adjustment of Rayleigh number

Rayleigh–Bénard Convection (RBC) is a common standardized model experiment for investigating thermal convection. It describes the heat and momentum transport due to thermally induced density gradients within a fluid, as it occurs e.g. in the atmosphere, oceans or the earth mantle. The boundary conditions are a heated bottom plate with uniform temperature T_H, a cooled top plate with uniform temperature T_C and adiabatic side-walls [4–6]. As the Prandtl number is independent from the scale, the dimensionless number to control RBC is the Rayleigh number Ra [7], which describes the temperature dependent flow patterning from a state where the fluid is at rest, over steady rolls via time-dependent patterns, to a fully turbulent state with increasing temperature [8]. The cubic dependency of Ra from the height of the experiment limits the application of large Ra for large Γ. Since the lateral expansion of the reality, i.e. atmosphere or oceans, is far away from experimental geometries that can be studied on a lab-scale, the experiment has to be scaled down, which means a dramatic

decrease of the experimental height and hence the Rayleigh number. That is why the height dependent change of Ra has to be compensated by the residual parameters entering the equation.

To keep the Rayleigh number constant for decreasing height of the experiment one could increase the temperature difference between the heating and cooling plate. There are two limitations: the temperature difference has to be moderate that the Oberbeck–Boussinesq approximation [2, 9, 10] (the density of the fluid is meant to be constant that the buoyancy force scales linearly with the temperature) is still valid, as well as the experimental setup itself cannot support "infinite" temperatures. As a rule of thumb, one has to satisfy $\beta\Delta T \lesssim 0.1$. The acceleration due to gravity is constant and does not play any role in adjusting Ra. Hence the fluid properties (kinematic viscosity ν, thermal diffusivity α, and thermal expansion β) have to be altered. A gas near its critical point, with a large thermal expansion coefficient, could be used as an option. Nonetheless, measurement of the velocity field by methods like PIV is rather complex and comes with many challenges for this method [9, 11]. Furthermore, the Prandtl number of gases at their critical point is generally high, therefore it is necessary to investigate when the Prandtl number is around 0.7. Another option is to change the fluid, e.g. the change from air to sulfur hexafluoride leads to an increase of Ra by about forty times at ambient conditions [12]. A larger change can be gained by compression of the fluid. Ra becomes larger when increasing the pressure. Hence the working fluid itself and the applied pressure are the main control parameters for adjusting Ra. A scaling factor m can be defined as the ratio of the characteristic length L_{ref} of a reference experiment to the desired characteristic length L of the scaled experiment, and is given by the following equation:

$$m = \frac{L_{\mathrm{ref}}}{L} = \left(\frac{\beta\nu_{\mathrm{ref}}\alpha_{\mathrm{ref}}}{\beta_{\mathrm{ref}}\nu\alpha}\right)^{\frac{1}{3}}. \tag{7}$$

In Figure 1(a), the desired pressure that has to be applied to achieve the corresponding scaling factor m of a scaled experiment for air and sulfur hexafluoride (SF_6) is exemplarily depicted. The corresponding values of the thermal expansion coefficient β, the kinematic viscosity ν, and the thermal diffusivity α were calculated for a mean temperature of $T = 298.15$ K, following the calculation rules for air [13, 14] and sulfur hexafluoride [15–17].

Figure 1(b) illustrates the parameter range of Ra that can be applied in the SCALEX for the presented Rayleigh–Bénard convection experiment with a height of 30 mm. The temperature range for the calculation of Ra was set from the minimum to the maximum applicable temperature difference ΔT to hold for the Oberbeck–Boussinesq approximation ($\beta\Delta T \leq 0.1$) [18]. However, in practice $\Delta T \leq 10$ K is necessary to ensure uniform temperature distribution in the cooling and heating plates.

3 The SCALEX facility

As the Rayleigh number is to be adjusted mainly by the fluid and the pressure, a closed vessel supports the application of larger pressures than the ambient pressure and separates the working fluid of the experiment from the ambient air,

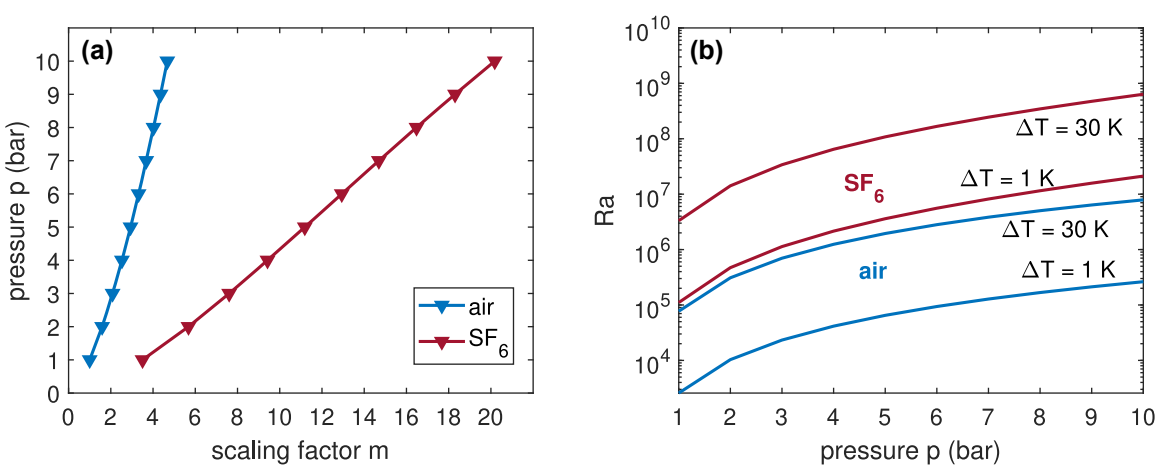

Figure 1: The pressure p that has to be applied for achieving the desired scaling factor m (a) and the parameter space of the Rayleigh number as a function of the applied pressure and temperature difference (b). Both calculations were applied for a mean temperature of $T = 298.15$ K for working fluids air and sulfur hexafluoride (SF_6). The convection cell height is 30 mm.

especially if the working fluid is environmentally harmful as sulfur hexafluoride [19]. As already mentioned the Prandtl number is independent of scale and is kept in the same range of air in natural convection, $\mathrm{Pr} \approx 0.7$ for air and $0.7 \leq \mathrm{Pr} \leq 1.3$ for SF_6. The vessel has to feature electrical access for connecting probes and sensors from the inside to the data acquisition system outside. Transparent windows guarantee access for optical measurements. Feedthroughs allow for water supply of the experimental setup as well as the heat exchanger inside the vessel for temperature control and the working fluid support. To meet this requirement the SCALEX facility is a cylindrical vessel with a permanently closed lid at the back and a removable lid at the front. Figure 2 shows a general overview and a technical drawing of the facility. SF_6 has a large greenhouse effect. Therefore, it is stored in a tank (orange tank in Figure 2) and delivered and extracted from the SCALEX via a compressor. Every time, the SCALEX is put under vacuum, and SF_6 is injected into it without mixing with air. Optical access is provided by five large flanges with borosilicate windows of a thickness of 40 mm and a diameter of 300 mm and 28 soda lime windows with a thickness of 20 mm and a diameter of 150 mm. The windows are evenly distributed and several smaller flanges allow for the installation of pressure probes and compressed-gas connection, one for dry air from the in house pressurized-air supply and one for the connection to the sulfur hexafluoride storage system, containing also a vacuum pump for evacuation of the vessel. The in-house air pressure supply delivers up to 9 bar and the sulfur hexafluoride pressurization system up to 4 bar, whereas the vessel is certified for working pressures of up to 10 bar above the ambient pressure.

3.1 Working pressure stability inside the SCALEX

The pressure has to be held constant for constant experimental conditions. There are two sources of pressure fluctuations. The first one (mechanical) is the leakage due to the manifold of flanges and the lids which necessitate exact and tight connection of all movable parts. Especially the transfer lid at the front of the vessel is to be well-adjusted to keep it tight. The second one (thermodynamical) is the change in volume of the vessel due to changes of the surrounding temperature as well as the gas expansion inside the vessel.

3.1.1 Mechanical influences

The leakage results in a pressure drop in the case of working pressures above the ambient pressure or a pressure increase if the working pressure is below the ambient pressure. Figure 3(a) depicts the pressure over time for air, starting with a working pressure of about 8.6 bar and 4.25 bar, respectively. The sinusoidal fluctuations along the linear decrease of the pressure originate from the thermodynamic effects by temperature fluctuations and will be discussed in the following paragraph. Anyhow, the pressure drop (slope of the linear fit function) is about 56.4 mbar/day or 2.35 mbar/h for the higher starting pressure and 13.7 mbar/day or 0.57 mbar/h for the lower starting pressure, respectively. Figure 3(b) shows the corresponding relative error $\Delta\mathrm{Ra}/\mathrm{Ra}$ of the Rayleigh number which is expected for a pressure drop of $\Delta p = 56$ mbar at a certain pressure p. The higher pressure value was chosen as worst case

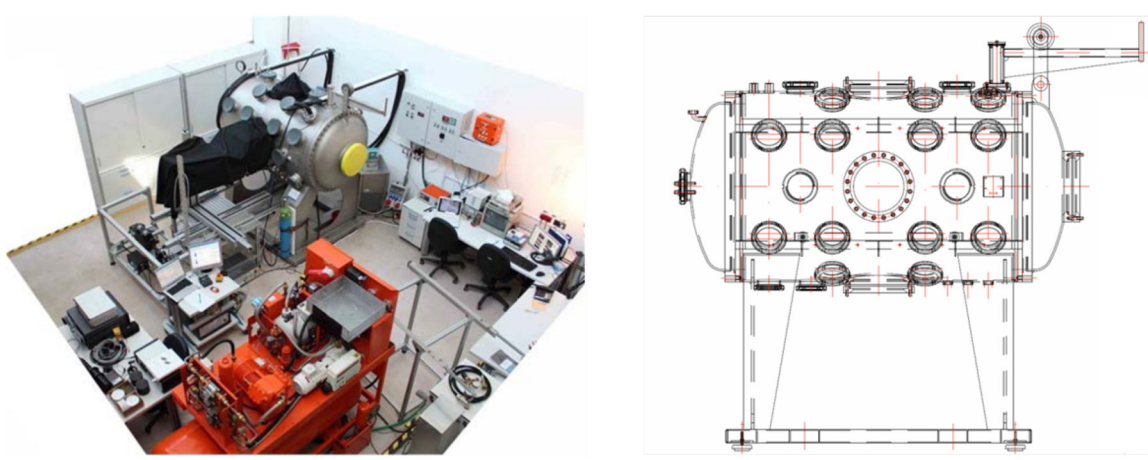

Figure 2: SCALEX facility, left: general overview of the facility and the storage tank for SF_6 in orange, right: technical drawing of the side view of the pressure vessel. Courtesy of Friedrich Wilhelm Heider GmbH, Behälter- und Apparatebau, Hillmicker Str. 28 + 30, 57482 Wenden, Germany. The diameter of the vessel is 1100 mm, total height is 2100 mm, and the length of facility (doors included) is 2200 mm.

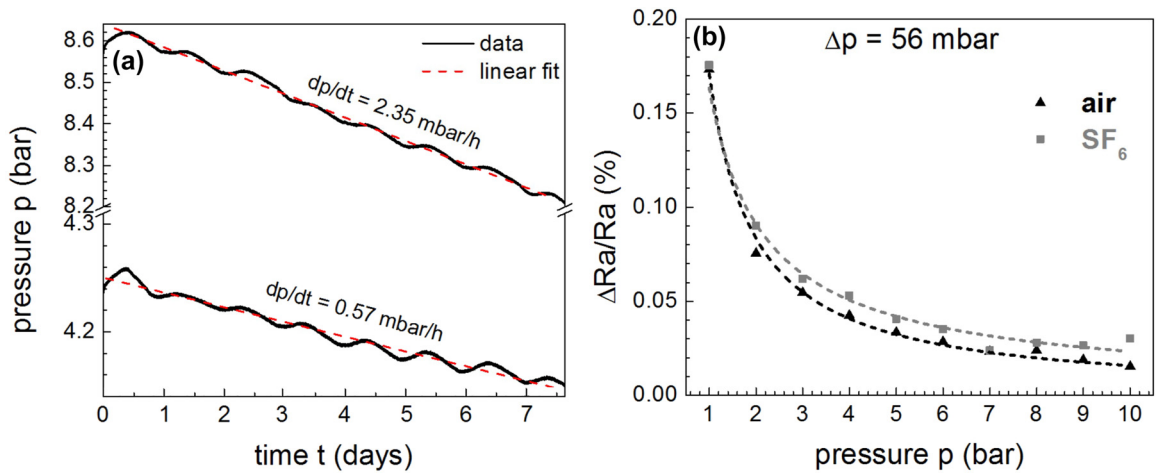

Figure 3: Pressure p as function of time t (a) and the corresponding relative error $\Delta\mathrm{Ra}/\mathrm{Ra}$ of the Rayleigh number for a pressure fluctuation of $\Delta p = 56$ mbar/day (b).

scenario, but only shows a relatively weak impact on the Rayleigh number.

3.1.2 Thermodynamic influences

The thermodynamic influences summarize the thermally induced effects, i.e., the thermal expansion of the gas as well as the thermal expansion of the vessel. The influence of the temperature fluctuation is simplified as follows. The diameter d and the length l of the cylindrical vessel depend on the thermal expansion coefficient β and the applied temperature difference ΔT_{SC} on the vessel (T_{SC} being the wall temperature of the vessel):

$$d = d_{\mathrm{ref}}(\beta\Delta T_{SC} + 1), \tag{8}$$

$$l = l_{\mathrm{ref}}(\beta\Delta T_{SC} + 1), \tag{9}$$

$$\Delta T_{SC} = T_{SC} - T_{SC_{\mathrm{ref}}}. \tag{10}$$

The reference values, d_{ref} and l_{ref}, are the values at a certain reference temperature $T_{SC_{ref}}$ were ΔT_{SC} is zero. The expanded volume V is then given by:

$$\begin{aligned} V &= \frac{\pi}{4} d^2 \cdot l \\ &= \frac{\pi}{4} d_{\mathrm{ref}}^2 (\beta\delta T_{SC} + 1)^2 \cdot l_{\mathrm{ref}}(\beta\delta T_{SC} + 1) \\ &= (\beta\Delta T_{SC} + 1)^3 \cdot V_{\mathrm{ref}}. \end{aligned} \tag{11}$$

By entering the assumed values into the van der Waals equation for a real gas

$$\frac{p + \frac{n^2 a}{V^2}(V - nb)}{T_{SC}} = \frac{\left(p_{\mathrm{ref}} + \frac{n^2 a}{V_{re} f^2}\right)(V_{\mathrm{ref}} - nb)}{T_{SC_{\mathrm{ref}}}} \tag{12}$$

and considering the amount of substance n as the ratio of the reference volume and the molar volume of the substance

$$n = \frac{V_{\mathrm{ref}}}{V_m} = \frac{V_{\mathrm{ref}}}{M} \tag{13}$$

the following equation is obtained for the pressure fluctuation $\Delta p = p - p_{\mathrm{ref}}$ as a function of temperature difference ΔT_{SC} at given reference values for pressure, temperature, and expansion coefficient, p_{ref}, $T_{SC_{\mathrm{ref}}}$ and β:

$$\begin{aligned} \Delta p = \Bigg\{ &\left(p_{\mathrm{ref}} + a\left(\frac{\rho}{M}\right)^2\right)\left(1 - \frac{\rho b}{M}\right)\left(\frac{\Delta T_{SC}}{T_{SC_{\mathrm{ref}}}} + 1\right) \ldots \\ &- \frac{a}{(\beta\Delta T_{SC} + 1)^3}\left(1 - \frac{\rho b}{M(\beta\Delta T_{SC} + 1)^3}\right) \\ &- \left(\frac{\rho}{M}\right)^2 \Bigg\} / \ldots \left\{(\beta\Delta T_{SC} + 1)^3 - \frac{\rho b}{M} - p_{\mathrm{ref}}\right\}. \end{aligned}$$

To visualize the influence of the thermal expansion, the pressure fluctuation Δp is plotted for stainless steel ($\beta = 16 \cdot 10^{-6}$ K^{-1}) exemplary at a reference temperature of $T_{SC_{\mathrm{ref}}} = 295$ K and a reference pressure of $p_{\mathrm{ref}} = 8$ bar, and multiples of β for comparison, see Figure 4. The van der Waals constants a and b for dry air are $a_{\mathrm{air}} = 0.1360$ N m^4 mol^{-2} and $b_{\mathrm{air}} = 3.657 \cdot 10^{-5}$ m^3 mol^{-1} and for sulfur hexafluoride $a_{\mathrm{SF6}} = 0.7857$ N m^4 mol^{-2} and $b_{\mathrm{SF6}} = 8.786 \cdot 10^{-5}$ m^3 mol^{-1}. The density at $p = 8$ bar and $T_{SC} = 295$ K is $\rho_{\mathrm{air}} = 9.475$ kg m^{-3} and $\rho_{\mathrm{SF6}} = 52.923$ kg m^{-3}, and the molar weight is $M_{\mathrm{air}} = 0.02896$ kg mol^{-1} and $M_{\mathrm{SF6}} = 0.14605$ kg mol^{-1}.

Due to the very small expansion coefficient β of stainless steel, there is only a marginal influence of the thermal expansion, and the expanding/shrinking volume of the

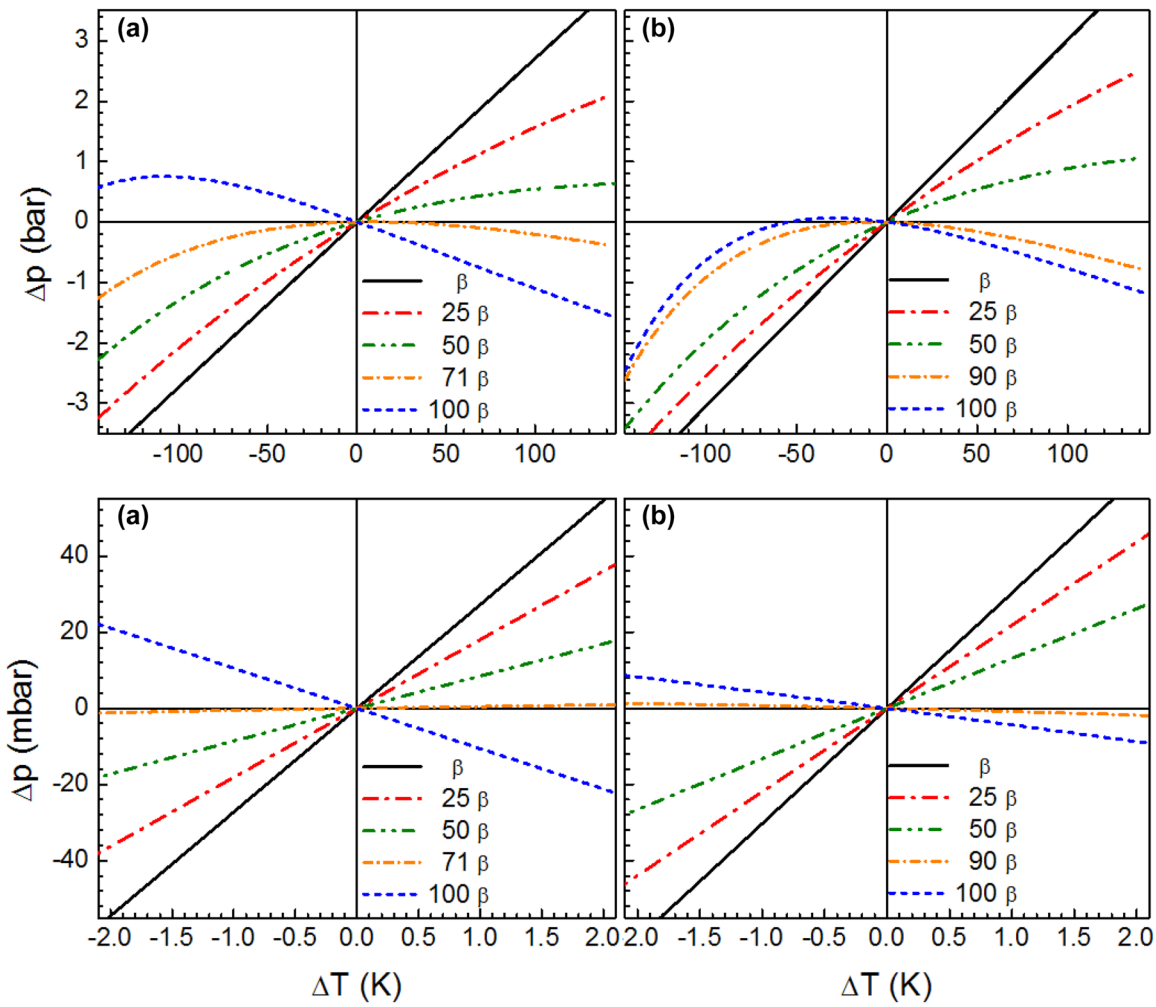

Figure 4: Calculated pressure fluctuation Δp of the SCALEX for air (a) and sulfur hexafluoride (b) as a function of the temperature fluctuation ΔT at a reference temperature of $T = 295$ K and a reference pressure of $p = 8$ bar. The top row depicts the pressure fluctuations over a wide temperature range, whereas the bottom row depicts the zoom-in region of the relevant temperature range for the working conditions of the SCALEX.

vessel can only slightly compensate for the temperature-induced pressure fluctuation of the gas. But, sulfur hexafluoride is slightly more susceptible to temperature fluctuations than air. Hence the pressure is dominantly influenced by the gas, i.e. volume fluctuations of the vessel can be neglected. From Figure 4 it can also be concluded that materials with an expansion coefficient of about 71 (90) times that of stainless steel would allow for compensation of the pressure fluctuations originating from the gas-air (sulfur hexafluoride) – within the relevant temperature range for the working conditions of the SCALEX. Thus the working conditions inside the vessel would be much more stable against temperature fluctuations if the thermal expansion coefficient of the construction material of the vessel fulfilled this requirement. But, since the vessel has to meet also the required mechanical stability and resistance against corrosion, other materials would not be applicable.

It is noteworthy that the pressure fluctuation for stainless steel is in the same range of about 50 mbar in the worst case as already discussed for the leakage of the vessel. Therefore, such low pressure fluctuations can be neglected as the impact on the Rayleigh number is very low (compare Figure 3(b)).

3.1.3 Stabilization of the working pressure and measurement conditions

The interior of the SCALEX is equipped with a heat exchanger to stabilize the mean temperature of the experiment. Figure 5 depicts the temperature fluctuations of the wall of the SCALEX, measured by eight evenly distributed thermal resistors (PT100) on the outer face of the wall,

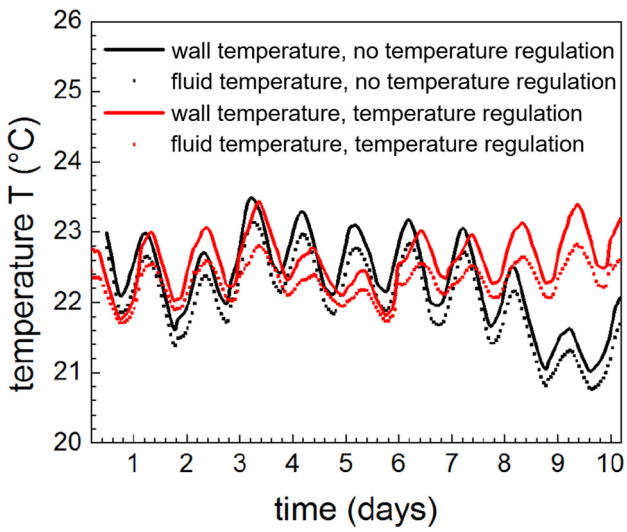

Figure 5: Temperature profile T as function of time t at the outer face of the wall and inside the SCALEX with and without temperature regulation.

and of the working fluid, measured by one thermal resistor (PT100) in the center of the vessel. Both temperatures were measured for two separate periods, one with temperature regulation and one without temperature regulation. Interestingly, the temperature shows a sinusoidal trend with a periodicity of one day. Hence the temperature fluctuations originate from the thermal fluctuations during day and night alterations. It is obvious that the temperature fluctuations of the wall and of the working fluid without temperature regulation are parallel translated with the same amplitude (degree of fluctuation). In contrast, the amplitude becomes slightly smaller in the working fluid than in the wall with temperature regulation. Thus the total temperature fluctuation within the working fluid is always below 1 K. Hence the pressure fluctuation is below 20 mbar (compare Figure 4). Furthermore, the measurement duration of a typical convection experiment does not exceed several hours. This implies that an evenly distributed measurement duration around the minimum or maximum of the curve, representing the daytime around afternoon and midnight, additionally minimizes the measurement error. But, when assuming the result for the total pressure fluctuation (compare Figure 3) where the thermally induced pressure fluctuation superposes the continuous pressure drop via leakage, favourable and unfavourable times for measurements with minimal pressure loss can be determined/derived.

3.2 Seeding stability

One of the most important factors guaranteeing valuable long-term particle-based velocity measurements is the successful generation and the stability of the airborne seeding particles under certain pressures. Therefore, seeding tests were conducted in the SCALEX in air with the commonly used DEHS (di(2-ethylhexyl) sebacate), vaporized with a Laskin nozzle, which results in a mean particle diameter of 1 µm [20]. The pressure for vaporization was established with an oil-free compressor. The generated particles were stored in a settling chamber, but not forwarded to the convection cell. It is worth mentioning that the entire seeding system, including the compressor are placed inside the SCALEX. The settling chamber was equipped with a photoelectric barrier (laser module plus photodiode) with top-down orientation to probe the relative change in particle concentration in the vertical cross-section over time. The seeding density is proportional to the photocurrent of the diode, absolute density values could not be obtained. Since the initial particle concentrations were different, the curves were normalized to the initial value. The normalized seeding concentration for various ambient pressures in air is depicted in Figure 6.

The seeding density drops very fast within the first minutes and then decays exponentially. This behavior can be explained by accelerated evaporation at large seeding densities, but then slows down when the density decreases. The seeding densities in the settling chamber are magnitudes larger than in the Rayleigh–Bénard convection experiment, where only little amounts are forwarded to the convection cell. Nonetheless, from the seeding experiment, one can conclude that the particle concentration is very stable for seeding densities typically applied in the convection experiment. Furthermore, the stability is sufficiently high

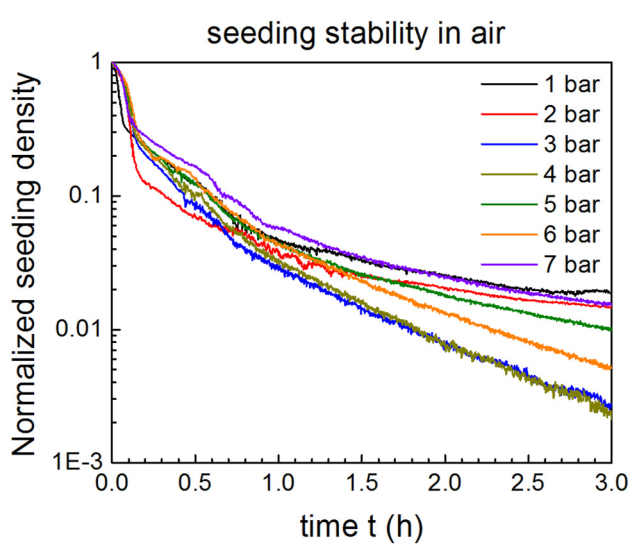

Figure 6: Normalized seeding density for various ambient pressures in air.

for all tested pressures and allows for measurement times of several hours without reseeding the experiment. However, the experimental setup is designed also for very sensitive reseeding in order to not disturb the convective flow during the measurement by continuously forwarding the seeding with very low flow rates.

4 Test experiment

4.1 Rayleigh–Bénard convection experiment inside SCALEX

Turbulent Rayleigh–Bénard convection was investigated in a closed cell with dimensions of $300 \times 300 \times 30$ mm^3 ($l \times l \times h$) inside the pressure vessel of the SCALEX facility, yielding an aspect ratio of $\Gamma = 10$. The transparent sidewalls were made of 4 mm thick polycarbonate, enabling illumination by a laser light sheet. The bottom edge of the sidewalls was chambered to reduce the contact area with the heating plate and prevent heat conduction through the sidewalls to the cooling plate. Hence, one sidewall was equipped with four countersunken PT100 (class B) resistance thermometers (UST Umweltsensortechnik GmbH), equidistantly distributed along the thermal gradient of the RB cell, to check the sidewall temperature distribution.

The transparent heating plate contains a heating pane of $500 \times 500 \times 4$ mm^3 size, one side coated with indium tin oxide (ITO) [21, 22]. Initially, it was necessary to stack two heating plates on top of each other in order to achieve uniform temperature distribution [21, 23–25]. However, by doing so, the light transmission through the plate was reduced significantly. A heating pane's light transmissivity is 0.68 [22], resulting in a total transmissivity of 0.4 for the entire heating plate. Consequently, this negatively affected the signal-to-noise ratio (SNR) of particle images. To solve this problem, instead of two a single heating pane with an improved uniform temperature distribution was manufactured. The plate was manufactured at the Fraunhofer Institute for Organic Electronics, Electron Beam and Plasma Technology FEP Dresden (Germany). Electrical contact was realized with spring strips from copper beryllium on the ITO surface. The heating power was controlled with an adjustable DC power supply (ELEKTRO-AUTOMATIK EA-PSI 9080-100). Figure 7 shows the temperature distribution over the heating plate captured by separate measurements using an infrared camera. During the measurement, the cooling plate was turned off. The average and standard deviation of the temperature distribution in the area of RBC over the heating plate are 28.63 °C and 0.36 K, respectively. In addition, the gradients from left to right and top to bottom

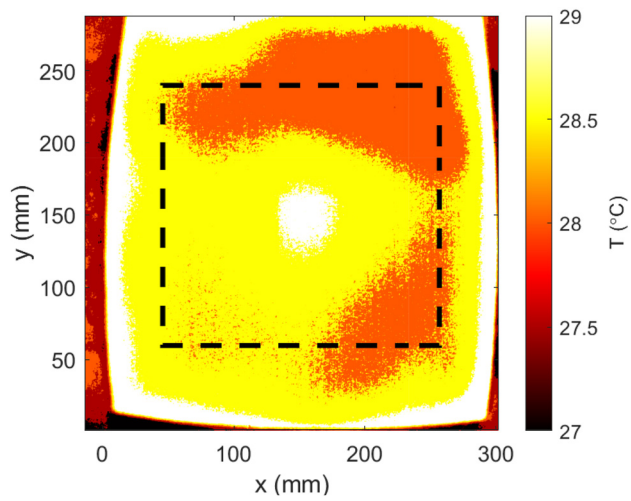

Figure 7: Temperature distribution over the heating plate. The area inside the dashed lines represents the field of view for PIV measurements.

are 0.60 K and 1.03 K, respectively, which is quite good and compares to former studies where two panes had to be applied to reach the same homogeneity [21, 23–25]. Using the current experiment as an example, the standard deviation to ΔT ratio will be 0.1. The non-transparent cooling plate (ELKOM ÖKOTHERM-PLUS) was driven by a recirculating cooler (Medingen C20 KB10). Surface temperatures were measured with four PT100 (class B) resistance thermometers (UST Umweltsensortechnik GmbH) at the cooling plate and four PT100 (class AA) resistance thermometers (TE Connectivity GmbH) at the heating plate close to the edges of the cell, about 20 mm away from the sidewalls. The PT100 sensors were fixed with two component thermally conductive adhesive (Phobya). The interior temperature of the SCALEX was regulated to the mean temperature of the convection experiment by a heat exchanger, driven by a recirculating cooler (Thermo Scientific HAAKE Phoenix II C40P). The working pressure was measured with a pressure sensor (Endress + Hauser AG Cera-bar PMC131). The outside wall temperature was measured with eight PT100 resistance thermometers, symmetrically distributed at the wall (UST Umweltsensortechnik GmbH). The internal ambient temperature was measured with one further PT100 resistance thermometer. The temperature sensors were four-wire sensed for the SCALEX, and three-wire sensed for the RBC. All sensor data (temperatures and pressure) were recorded with a data logging system (National Instruments Corporation: NI PXI-1033, NI PXI-4071, NI TB-2633) for the RBC and Agilent 34972A for the SCALEX. All devices (chillers, power supply, data logger) were controlled via LabVIEW software.

4.2 Particle image velocimetry

The velocity fields were obtained by stereoscopic Particle Image Velocimetery (PIV) [26] in the horizontal mid-plane of the cell. The 3 mm thick laser light sheet was created with a double pulse laser (Quantel Q-smart Twins 850) with approx. 300 mJ pulse energy, equipped with light sheet optics. The experiments were done using double frame recording at various frame rates and pulse separation times according to the flow velocity. The images were recorded with two sCMOS cameras (LaVision Imager sCMOS), with $6.5 \times 6.5\ \mu m^2$ pixel size, equipped with Zeiss Distagon f 50 mm objective lenses. Figure 8 shows a schematic sketch of the experimental setup inside the SCALEX. Due to space reasons, cameras are looking through a mirror tilted 45° with respect to the heating plate. The image magnification factor is $M = 0.08$. The f stop for the cameras is 4 and 2.8 for forward and backward scattering for the cameras in right and left of the Figure 8, respectively. In order to ensure their functionality under higher pressures and in the case of an evacuation of the facility during experiments with SF_6, the cameras were tested under vacuum and pressures up to 6 bar. In previous experiments, the cameras were located outside the SCALEX facility, and glass windows provided optical access beneath the facility [21, 23]. However, this limited the stereoscopic angle to about 20°, creating a significant bias for in-plane displacements during the measurements. The cameras are therefore moved to the inside of the vessel to increase the stereoscopic angle, reduce the optical barrier, and thus increase the SNR as well [25]. The stereoscopic angle between the two cameras is about 40°, and Scheimpflug condition was applied to the cameras to maintain ideal focus in the entire field of view. However, this was at the expense of an increase in the leakage of the SCALEX due to the adjustments done in one of the flanges for the connection of the cameras with the optical fibers out side the pressure vessel. The pressure drop for the current experiment at $p = 4.5$ bar was about 14 mbar/h, which is still relatively low considering the fact that the measurement time was only a quarter of an hour, and results in $\Delta Ra/Ra \approx 2 \times 10^{-3}$ for the entire measurement. Laser and the cameras were synchronized by a programmable timing unit (LaVision PTU X), connected to a computer controlled by the DaVis 10 software (LaVision GmbH).

The seeding was generated with a vaporizer (PIVpart12, PIVTEC GmbH) and consisted of small ($O \approx 1\ \mu m$) droplets of di(2-ethylhexyl) sebacate (DEHS). The seeding generator was placed inside the pressure vessel. The pressure difference against the ambient pressure inside the SCALEX was applied with a compressor (Jun Air OF301 4B), also placed inside the vessel. The seeding was first injected into a large settling chamber ($300 \times 300 \times 300\ mm^3$). After a full charge, the seeding was forwarded to the convection cell by six distributed ports with very low pressure, generated with a very low flow rate fan, to not push the natural flow with an additional momentum by the seeding injection. The whole process of seeding generation, injection to the settling chamber, and injection to the convection cell was externally controlled with magnetic valves. A schematic of the seeding system is sketched in Figure 9. To avoid bias in the measurements from the seeding injection, data acquisition was started at 15 min after injection, when the natural

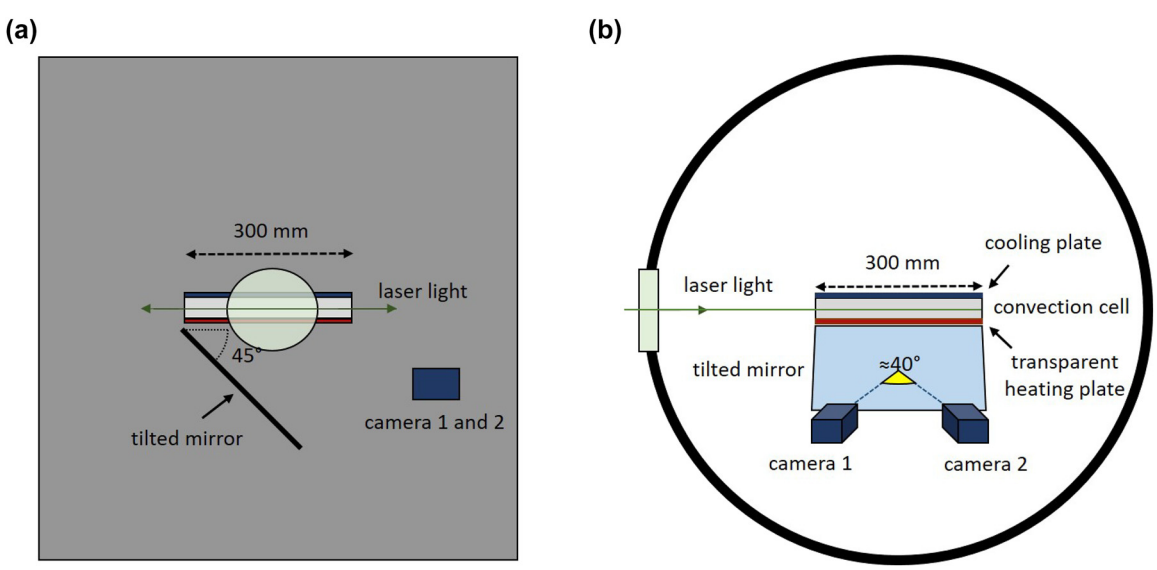

Figure 8: A schematic sketch of SCALEX facility and the convection cell, the side view (a), and the front view (b).

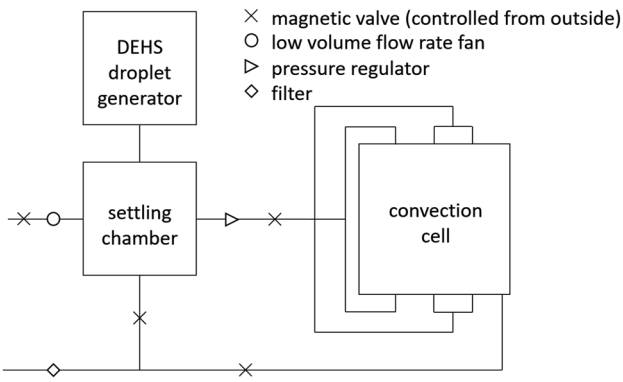

Figure 9: Schematic of the seeding injection principle.

convection flow is already fully established. To ensure the faithful following of the flow by the tracer particles in the current experiment, the Stokes number was calculated as follow:

$$St = \frac{d_p \rho_p u_f}{18 \eta g} < 10^{-2} \tag{14}$$

With d_p being the particle diameter, ρ_p the particle density, η the dynamic viscosity, u_f the free-fall velocity. The free fall velocity is the speed of fast convective motion $u_f = \sqrt{\beta \Delta T g h}$. The calibration was conducted with a 3D calibration plate (200×200 mm^2, LaVision GmbH). The calibration plate was placed in the center position at mid-plane of the convection experiment inside the SCALEX and a pin-hole model was applied to map the coordinate system. Additionally, a stereoscopic self-calibration was performed to further reduce errors in the calibration [27].

Image processing was performed with a commercial software package (DaVis 10, LaVision GmbH). The time-averaged image of the 10,000 images of the entire experiment (which is calculated for all captured images) was subtracted from each individual image to increase contrast and remove the background. The preprocessed images were evaluated with a decreasing interrogation window size, starting at 96×96 pixels with 50% overlap and ending at 48×48 pixels (three further passes) with 75% overlap. The field of view covered $7h \times 6h$, and the final spatial resolution was 1.03×1.03 mm^2 in physical coordinates with 206×173 vectors. Further details on the setup and the specific tasks for reliable PIV measurements in RB flows can be found in Cierpka et al. (2019) [23].

4.3 Results

In this section, the results of a sample experiment for Rayleigh–Bénard Convection (RBC) in air for Ra $= 1.9 \times 10^5$ and Pr $= 0.7$ are presented. Table 1 shows the parameters of the current experiment. The experiment was conducted for 2000 free-fall times t_f with a measurement frequency of 10 Hz resulting in a total of 10,000 snapshots. The free fall time is equal to $t_f = h/u_f$ where u_f is the speed of fast convective motion $u_f = \sqrt{\beta \Delta T g h}$. Figure 10 shows the measurement results. The instantaneous velocity field is displayed in Figure 10(a). The color map represents the out-of-plane velocity component normalized by the free fall velocity w/u_f with the positive direction being from the heating plate towards the cooling plate. The upward hot and downward cold flow is visible in red and blue respectively, and the direction of the in-plane movement is indicated by vectors. No post-processing has been applied to the data.

The Probability Density Functions (PDF) of all three velocity components are shown in Figure 10(b). The PDFs are for the entire measurement period of 2000 t_f. Comparable numerical results for this range of Rayleigh numbers are limited to less than 100 t_f [28]. Due to the very small diameter of the seeding particles and the particle images as a result, peak locking was a point of concern for the current experiment [29]. However, there was no sign of peak locking in the displacement distributions. The two in-plane components, u and v, have symmetric Gaussian distributions which almost overlap with each other. Therefore, one can argue that the nature of the turbulent flow is identical in the two in-plane directions. For the out-of-plane velocity component, the PDF distribution is relatively flat at zero. Furthermore, the distribution is not completely symmetric between negative and positive values. This might be due to several possible reasons. One possibility is that the relatively small aspect ratio of the cell affects the flow structure in a way that the measurement plane position will slightly affect the out-of-plane velocity distribution. The second possible reason might be that this slight asymmetry is a feature of the flow itself. Finally, the experimental nature of the

Table 1: Parameters for the current experiment in the Rayleigh–Bénard cell.

Ra	P	ΔT	T_H	Free-fall velocity u_f	Free-fall time t_f	No. of images	Measurement time in t_f
1.9×10^5	4.5 bar	3.6 K	26.8 °C	60 mm/s	0.5 s	10,000	2000

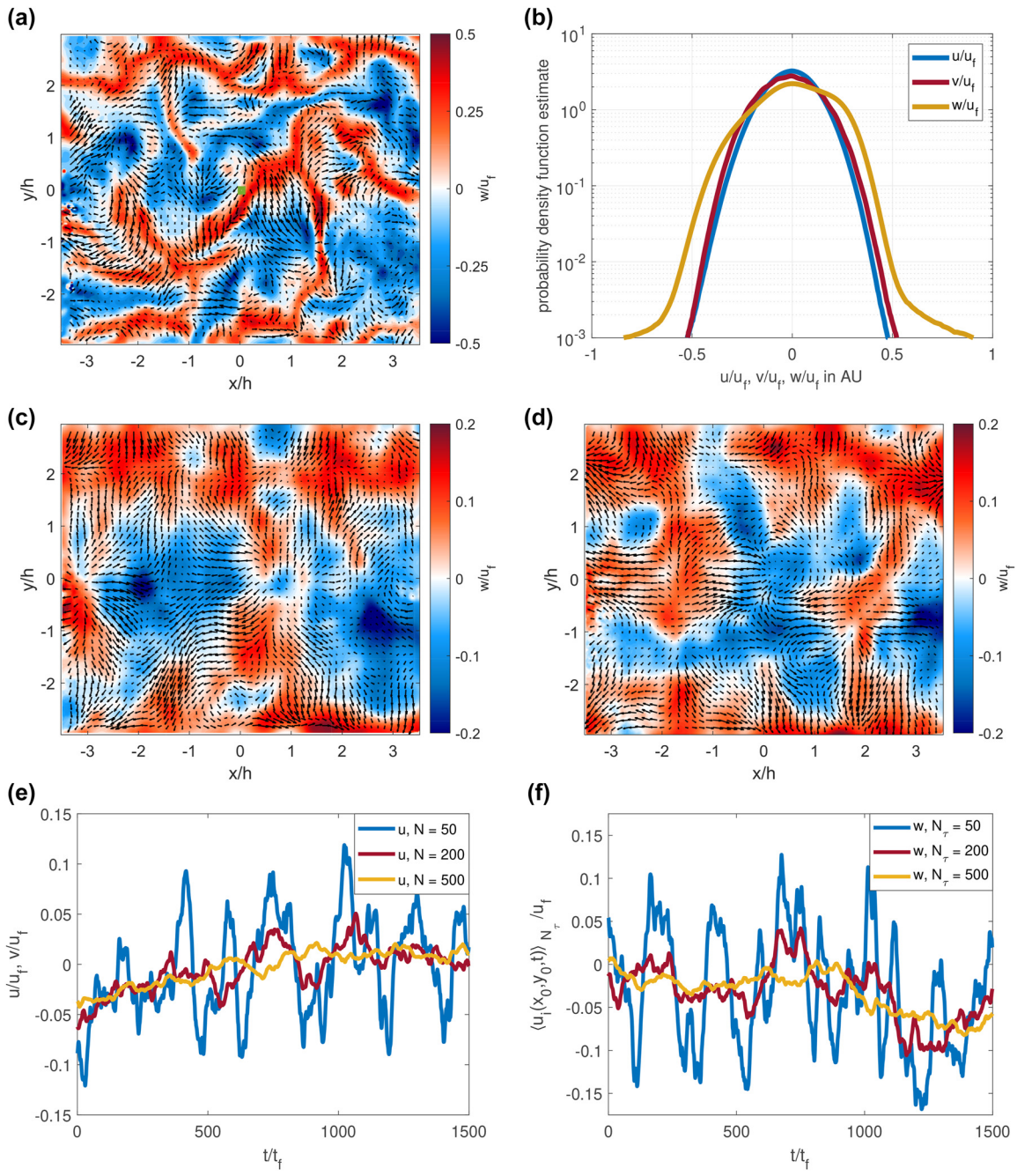

Figure 10: The results of the PIV measurements for Ra $= 1.9 \times 10^5$, the instantaneous velocity field (a), the probability density function (PDF) estimate of three velocity components (b), time-averaged velocity field for (0–100) t_f (c), time-averaged velocity field for (1500–1600) t_f (d), evolution of the mean value for the horizontal in-plane velocity component u for three different moving mean window sizes of $N_\tau = 50, 200, 500\ t_f$ (e), and evolution of the mean value for the out-of-plane velocity component w for three different moving mean window sizes of $N_\tau = 50, 200, 500\ t_f$ (f).

data forces us to encounter some inevitable imperfections compared to numerics [30], which might also contribute to this asymmetric profile of the PDF distribution for the out-of-plane velocity component. For example, the cell is rather thin (30 mm), so the asymmetries in the PDF might be caused by the image plane not lying exactly at mid-height.

The patterns are already visible in the instantaneous velocity field, and it seems that their dimensions are of the same order of magnitude as the field of view itself. Previously, it was shown that the superstructures of turbulent convection are visible in a time-averaged flow for a period of around 100 t_f, and these superstructures

reorganize in about $1500t_f$ [28]. Therefore, the time-averaged velocity field for the first and sixteenth $100t_f$ are shown in Figure 10(c) and (d), respectively. Clearly, superstructures are present in the flow, but their dimensions are around $5h \times 5h$ and probably only 4 or 5 of them are present in the entire $10h \times 10h$ convection cell. Furthermore, 1500 t_f is a sufficient time span for the reorganization of the superstructures, since the patterns are completely different for the two time-averaged velocity fields, as can be seen by the low correlation coefficient of 0.27 for the out-of-plane velocity component w [31].

Figure 10(e) and (f) show the evolution of the mean value of the in-plane and out-of-plane velocity components for a single point in the field of view, respectively. Due to the similarity of the in-plane velocity components, only u is preselected. The position of the respective point is shown by a green square in Figure 10(a). The temporal mean values are calculated for three different moving time spans of $N_\tau = 50, 100$, and $500t_f$:

$$\langle u_i(x_0, y_0, t)\rangle_{N_\tau} = \frac{1}{N_\tau} \sum_{t_i=-\frac{N_\tau}{2}}^{\frac{N_\tau}{2}} u_i(x_0, y_0, t + t_i) \tag{15}$$

The location of the averaged point is $x_0 = 0.03$ h and $y_0 = 0$ h, and its marked in green in the center of Figure 10(a). All three velocity components have similar trends in their fluctuations. For $N_\tau = 50t_f$ the fluctuations are significant, but as the time span N_τ increases they converge to constant values. However, the values are still fluctuating even for the largest window size of $N_\tau = 500$. Thus, in order to acquire fully dynamically resolved data, much longer measurement periods are required to capture several reorganizations of the superstructures. This task is left as a future work.

In general, the results show that the SCALEX facility can be used for experiments of Rayleigh–Bénard convection at higher pressures for a reasonably extended period of time to provide statistics of the turbulent flow that is convergent with respect to time. The optical access through the heating plate was a major challenge which was addressed successfully by the movement of the cameras to the inside of the facility and using a transparent heating plate with a single heating pane model in order to reduce the optical barriers.

5 Summary

We presented an apparatus for fluid mechanical experiments in a reduced-scale model room, including convection. As a result, it reaches the functionality of many expensive full-scale investigations and provides a comprehensive tool for generating accurate data for evaluating numerical methods. SCALEX has the advantage of having shorter time scales than spatially full-scale experiments. In contrast to full-scale experiments that can take days or weeks to complete, in the SCALEX facility it takes only an hour to conduct convection experiments for several thousand free fall time units. The abilities of the SCALEX facility go far beyond the investigation of standard Rayleigh–Bénard convection experiments and will play an important role in a broad range of future studies like indoor air-flow problems, which was the original intention of the SCALEX [32, 33]. Finally, the SCALEX facility allowed for the first time detailed optical flow measurements of convection in compressed gases so far and hence paves the way to new insights into natural and forced convection problems and related structure formation.

Author contributions: All the authors have accepted responsibility for the entire content of this submitted manuscript and approved submission.

Research funding: Funding of this work by the Deutsche Forschungsgemeinschaft (DFG) within the Priority Programme DFG-SPP 1881 “Turbulent Superstructures” and by the Carl Zeiss Foundation within the project no. P2018-02-001 “Deep Turb–Deep Learning in and of Turbulence” is acknowledged. The work of Valentina Valori was supported by the Marie Skłodowska-Curie Fellowship of the European Union with Project No. 101024531.

Conflict of interest statement: The authors declare no conflicts of interest regarding this article.

References

[1] E. Buckingham, “On physically similar systems; illustrations of the use of dimensional equations,” *Phys. Rev.*, vol. 4, pp. 345—376, 1914.

[2] H. Yik, V. Valori, and S. Weiss, “Turbulent Rayleigh—Bénard convection under strong non-Oberbeck-Boussinesq conditions,” *Phys. Rev. Fluids*, vol. 5, p. 103502, 2020.

[3] H. Herwig, *Strömungsmechanik*, Berlin, Heidelberg, Springer, 2006.

[4] H. Bénard, “Les tourbillons cellulaires dans une nappe liquide-méthodes optiques d’observation et d’enregistrement,” *J. Phys. Theor. Appl.*, vol. 10, pp. 254—266, 1901.

[5] S. Ostrach, “Natural convection in enclosures,” *J. Heat Transfer*, vol. 110, pp. 1175—1190, 1988.

[6] L. Rayleigh, “On convection currents in a horizontal layer of fluid, when the higher temperature is on the under side,” *Lond. Edinb. Dublin Philos. Mag. J. Sci.*, vol. 32, pp. 529—546, 1916.

[7] H. Jeffreys, “The stability of a layer of fluid heated below,” *Lond. Edinb. Dublin Philos. Mag. J. Sci.*, vol. 2, pp. 833—844, 1926.

[8] M. C. Cross and P. C. Hohenberg, “Pattern formation outside of equilibrium,” *Rev. Mod. Phys.*, vol. 65, pp. 851—1112, 1993.

[9] V. Valori, G. E. Elsinga, M. Rohde, J. Westerweel, and T. H. van Der Hagen, “Particle image velocimetry measurements of a thermally

convective supercritical fluid," *Exp. Fluids*, vol. 60, pp. 1—14, 2019.
[10] V. Valori, G. Elsinga, M. Rohde, M. Tummers, J. Westerweel, and T. van der Hagen, "Experimental velocity study of non-Boussinesq Rayleigh—Bénard convection," *Phys. Rev. E*, vol. 95, p. 053113, 2017.
[11] D. Threlfall, "Free convection in low-temperature gaseous helium," *J. Fluid Mech.*, vol. 67, pp. 17—28, 1975.
[12] M. Wedi, D. P. Van Gils, E. Bodenschatz, and S. Weiss, "Rotating turbulent thermal convection at very large Rayleigh numbers," *J. Fluid Mech.*, vol. 912, 2021, https://doi.org/10.1017/jfm.2020.1149.
[13] K. Kadoya, N. Matsunaga, and A. Nagashima, "Viscosity and thermal conductivity of dry air in the gaseous phase," *J. Phys. Chem. Ref. Data*, vol. 14, pp. 947—970, 1985.
[14] E. W. Lemmon, R. T. Jacobsen, S. G. Penoncello, and D. G. Friend, "Thermodynamic properties of air and mixtures of nitrogen, argon, and oxygen from 60 to 2000 K at pressures to 2000 MPa," *J. Phys. Chem. Ref. Data*, vol. 29, pp. 331—385, 2000.
[15] C. Guder and W. Wagner, "A reference equation of state for the thermodynamic properties of sulfur hexafluoride (SF_6) for temperatures from the melting line to 625 K and pressures up to 150 MPa," *J. Phys. Chem. Ref. Data*, vol. 38, pp. 33—94, 2009.
[16] J. Kestin and N. Imaishi, "Thermal conductivity of sulfur hexafluoride," *Int. J. Thermophys.*, vol. 6, pp. 107—118, 1985.
[17] J. Hoogland, H. Van Den Berg, and N. Trappeniers, "Measurements of the viscosity of sulfur hexaflouride up to 100 bar by a capillary-flow viscometer," *Physica A*, vol. 134, pp. 169—192, 1985.
[18] D. D. Gray and A. Giorgini, "The validity of the Boussinesq approximation for liquids and gases," *Int. J. Heat Mass Transfer*, vol. 19, pp. 545—551, 1976.
[19] C. T. Dervos and P. Vassiliou, "Sulfur hexafluoride (SF_6): Global environmental effects and toxic byproduct formation," *J. Air Waste Manage. Assoc.*, vol. 50, pp. 137—141, 2000.
[20] C. Kähler, B. Sammler, and J. Kompenhans, "Generation and control of tracer particles for optical flow investigations in air," *Exp. Fluids*, vol. 33, pp. 736—742, 2002.
[21] C. Kästner, C. Resagk, J. Westphalen, M. Junghähnel, C. Cierpka, and J. Schumacher, "Assessment of horizontal velocity fields in square thermal convection cells with large aspect ratio," *Exp. Fluids*, vol. 59, pp. 1—13, 2018.
[22] D. S. Ginley and C. Bright, "Transparent conducting oxides," *MRS Bull.*, vol. 25, pp. 15—18, 2000.
[23] C. Cierpka, C. Kästner, C. Resagk, and J. Schumacher, "On the challenges for reliable measurements of convection in large aspect ratio Rayleigh—Bénard cells in air and sulfur-hexafluoride," *Exp. Therm. Fluid Sci.*, vol. 109, p. 109841, 2019.
[24] V. Valori, A. Thieme, C. Cierpka, and J. Schumacher, "Rayleigh—Bénard convection in air: out-of-plane vorticity from stereoscopic PIV measurements," in *14th International Symposium on Particle Image Velocimetry*, vol. 1, 2021.
[25] V. Valori, R. Kräuter, and J. Schumacher, "Extreme vorticity events in turbulent Rayleigh—Bénard convection from stereoscopic measurements and reservoir computing," *Phys. Rev. Res.*, vol. 4, p. 023180, 2022.
[26] A. K. Prasad, "Stereoscopic particle image velocimetry," *Exp. Fluids*, vol. 29, pp. 103—116, 2000.
[27] B. Wieneke, "Stereo-PIV using self-calibration on particle images," *Exp. Fluids*, vol. 39, pp. 267—280, 2005.
[28] A. Pandey, J. D. Scheel, and J. Schumacher, "Turbulent superstructures in Rayleigh—Bénard convection," *Nat. Commun.*, vol. 9, p. 2118, 2018.
[29] R. J. Adrian and J. Westerweel, *Particle Image Velocimetry*, Cambridge: Cambridge University Press, 2011, p. 30.
[30] S. Moller, T. Käufer, A. Pandey, J. Schumacher, and C. Cierpka, "Combined particle image velocimetry and thermometry of turbulent superstructures in thermal convection," *J. Fluid Mech.*, vol. 945, p. A22, 2022.
[31] S. Sachs, M. Baloochi, C. Cierpka, and J. König, "On the acoustically induced fluid flow in particle separation systems employing standing surface acoustic waves—part i," *Lab Chip*, vol. 22, pp. 2011—2027, 2022.
[32] M. Körner, "An experimental method for the investigation of indoor airflows in a reduced scale model room: development and application," Ph.D. thesis, TU Ilmenau, 2014.
[33] M. Körner, O. Shishkina, C. Wagner, and A. Thess, "Properties of large-scale flow structures in an isothermal ventilated room," *Build Environ.*, vol. 59, pp. 563—574, 2013.

Bionotes

Mohammad Sharifi Ghazijahani
Institute of Thermodynamics and Fluid Mechanics, Technische Universität Ilmenau, P. O. Box 100565, 98693 Ilmenau, Germany
mohammad.sharifi-ghazijahani@tu-ilmenau.de

Mohammad Sharifi Ghazijahani graduated from Sharif University of Technology in Iran in 2016 with a Bachelor's degree in Aerospace engineering. He continued his studies in Mechanical engineering at the Middle East Technical University in Turkey till 2019. Currently, he is a scientific researcher at the Institut für Thermo- und Fluiddynamik of Technische Universität Ilmenau on experimental fluid dynamics and machine learning analysis of experimental data in pursuit of his Ph.D. He is interested in flow control, turbulence, optical flow measurement techniques, and machine learning.

Christian Kästner
Institute of Thermodynamics and Fluid Mechanics, Technische Universität Ilmenau, P. O. Box 100565, 98693 Ilmenau, Germany

Christian Kästner studied engineering physics at the Technische Universität Ilmenau until 2008. From 2008 to 2010, he was research assistant at the Leibniz Institute for Solid State and Materials Research Dresden. In 2010, he started working as a research assistant at the Institute of Physics at the Technische Universitäat Ilmenau, receiving his doctorate in experimental physics in 2014. Until 2019, he worked as research assistant at the Institute of Thermodynamics and Fluid Mechanics at the Technische Universitäat Ilmenau. In 2019, he joined the

Production Technology Group, working in the field of laser beam welding. In 2021, he became research assistant in the Aerodynamics Group, continuing his work in turbulent Rayleigh-Bénard convection.

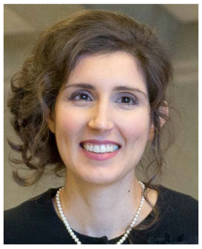

Valentina Valori
Institute of Thermodynamics and Fluid Mechanics, Technische Universität Ilmenau, P. O. Box 100565, 98693 Ilmenau, Germany

Valentina Valori holds a Master degree in Energy Engineering from the University of Pisa, and a Ph.D. in Fluid Mechanics from the Delft University of Technology. She worked as Postdoc at the Fundamental Research Division of CEA from 2018 to 2020, and as Postdoc with a Marie Sk lodowska-Curie fellowship in the Fluid Mechanics group at the Technische Universität Ilmenau from 2020 to 2022. Since September 2022 she works as Researcher in the Nuclear Safety Multiphase Flows group at ETH Zürich. Her research interests are turbulence, thermal convection, and experimental techniques in fluid mechanics.

Alexander Thieme
Institute of Thermodynamics and Fluid Mechanics, Technische Universität Ilmenau, P. O. Box 100565, 98693 Ilmenau, Germany

Alexander Thieme finished his bachelor degree in physics engineering at Ernst-Abbe-Hochschule Jena. Afterwards he worked as a control engineer for Tadano Faun GmbH. Since 2010 he is employed at Technische Universität Ilmenau. He is responsible for the SCALEX and supports the ongoing research in this facility. His research interests range from convection phenomena to optical flow measurements.

Kerstin Täschner
Fraunhofer Institute for Organic Electronics, Electron Beam and Plasma Technology FEP Dresden, Winterbergstraße 28, 01277 Dresden, Germany

Kerstin Täschner studied Optometry at the Dept. Precision engineering of University of Applied Sciences Jena and finished her Dipl.-Ing. in 2002. Afterwards she specialized in optical thin film deposition by plasma ion-assisted vacuum evaporation at Fraunhofer IOF Jena and defended her doctoral thesis about optical coatings on polymer substrate in 2006 at Martin-Luther-University Halle-Wittenberg/ Dept. Engineering science. Since 2006 she works in the field of reactive magnetron sputtering at Fraunhofer FEP Dresden and is the leader of the sheet-tosheet Sputtering PECVD research group. Her main research interests are multifunctional optical coatings, flexible thin glass and optical metrology.